



NUMERICAL ANALYSIS OF A WATER HEATING SYSTEM USING A FLAT PLATE SOLAR COLLECTOR

ANÁLISIS NUMÉRICO DE UN SISTEMA DE CALENTAMIENTO DE AGUA UTILIZANDO UN COLECTOR SOLAR DE PLACA PLANA

William Quitiaquez^{1,*}, José Estupiñán-Campos², C. A. Isaza-Roldán¹,
 Fernando Toapanta-Ramos², Andrés Lobato-Campoverde²

Abstract

The objective of the present research work was to carry out a numerical analysis by means of CFD of a flat plate solar collector, in addition to a comparison with experimental results. The working fluid reached a maximum outlet temperature of 20.16 °C at 12:00, the value of solar radiation was determined for the geographical coordinates latitude -0.2252 and longitude -77.84; similarly, at this time it was possible to obtain a temperature of 27.12 °C on the collector surface, as peak value. The lowest performance of the heat transfer device was determined at 10:00 with an outlet water temperature and maximum temperature on the collector surface of 18.65 and 20.48 °C, respectively. The experimental results showed a maximum temperature of 20.93 °C and a minimum temperature of 19.4 °C, resulting in a 4.01 % error between the computational simulation and the experimental data.

Keywords: Collector, solar energy, temperature, CFD simulation.

Resumen

El objetivo de la presente investigación fue realizar un análisis numérico mediante CFD de un colector solar de placa plana; además, se realizó una comparación con resultados experimentales. El fluido de trabajo alcanzó una temperatura máxima de salida de 20.16 °C a las 12:00, el valor de la radiación solar se determinó para las coordenadas geográficas latitud -0.2252 y longitud -77.84; de forma similar, en este horario fue posible obtener una temperatura de la superficie del colector de 27.12 °C, como valor pico. Se determinó el menor rendimiento del dispositivo de transferencia de calor a las 10:00 con un valor de temperatura de salida del agua y temperatura máxima en la superficie del colector de 18.65 y 20.48 °C, respectivamente. Los resultados experimentales mostraron una temperatura máxima de 20.93 °C y una temperatura mínima de 19.4 °C, derivando en un error de 4.01 % entre la simulación computacional y los datos experimentales.

Palabras clave: colector, energía solar, temperatura, simulación CFD

^{1,*}Centro de Investigación en Refrigeración y Aire Acondicionado, Universidad Pontificia Bolivariana, Colombia.
 Corresponding author ✉: william.quitiaquez@upb.edu.co.

<https://orcid.org/0000-0001-9430-2082>, <https://orcid.org/0000-0002-5902-6411>

²Carrera de Ingeniería Mecánica / GIERIMP, Universidad Politécnica Salesiana, Quito, Ecuador.

<https://orcid.org/0000-0003-2286-5737>, <https://orcid.org/0000-0002-0838-4702>,

<https://orcid.org/0000-0002-6073-3439>.

Received: 16-05-2020, accepted after review: 12-06-2020

Suggested citation: Quitiaquez, W.; Estupiñán-Campos, J.; Isaza-Roldán, C. A.; Toapanta-Ramos, F. and Lobato-Campoverde, A. (2020). «Numerical Analysis of a Water Heating System Using a Flat Plate Solar Collector». *INGENIUS*. N.º 24, (july-december). pp. 97-106. DOI: <https://doi.org/10.17163/ings.n24.2020.10>.

1. Introduction

At present, it has been observed how the scientific community has become aware about the use of energy renewable sources, due to many studies about the damages produced by the burning of fossil fuels for the generation and use of energy. For this reason, in recent years there has been an increase in the research and experimental works about the use of solar energy for increasing the temperature of fluids using thermal solar collectors; among them there are the concentrating solar collectors which have determined that the operating range varies between 50 and 300 °C [1].

Taking advantage of this virtually renewable resource has more impact in places with an appropriate geographic location to optimize the performance of heat transfer devices with the assistance of solar energy, due to the appropriate and invariant angle of incidence by the influence of the seasons, as it is the case of countries in the equatorial region such as Ecuador [2].

Ayompe and Duffy [3], in their research work about the thermal performance of a water heating solar system with flat plate collectors applied along one year at a forced circulation household scale system, show that the obtained results corresponded to a yearly average of collected daily energy of 19.6 MJ/day, a solar fraction of 32.2 %, and, in addition, a collector and system efficiency of 37.8 and 45.6 %, respectively.

There are various external agents involved in the operation of a solar collector, namely the ambient temperature, irradiation, geographic position, among others, as stated by Hashim *et al.* [4]. In their work they show the influence of the volumetric flow in the temperature that the working fluid may reach when leaving the solar collector; in their experimental research they conducted two tests with flow rates of 5.3 and 6.51 L·min⁻¹, respectively, obtaining as results output temperatures of 51.4 and 49 °C, reaching the conclusion that as the volumetric flow rate decreases a greater temperature may be reached at the outlet of the collector.

The Computational Fluid Dynamics (CFD) is of great help in studies that seek to improve the performance of heat transfer devices. For this reason it is regularly used to develop improved designs of various mechanisms that require energy transfer, such as solar

air heaters, and to evaluate the potential of power generation [5].

In their research, Marroquín *et al.* [6] use the ANSYS simulation software, specifically its library for fluid dynamics (CFD). The CFX-Mesh is utilized for the meshed, where it is considered a face space in the elements between 0.004 and 0.08 m, a resolution angle of 30°; regarding the simulation, it is carried out under the k-epsilon energy model due to the turbulent flow, obtaining a result that varies 5% with respect to the experimentation.

It is possible to perform a comparative analysis to validate the results of the CFD analysis with experimental results seeking to find a permissible error margin as stated by Mohamed *et al.* [7], who in their study of a Direct Expansion Solar Assisted Multifunctional Heat Pump (DX-SAMHP) take real parameters such as external ambient temperature during winter from -1 to 5 °C, solar radiation of 0, 57, 100 and 200 W·m⁻² to enter them in the simulator, obtaining larger values in the modeling compared to the experimental results, with average deviations of ± 4 %.

Similarly, the research work by Duarte *et al.* [8] presents a comparative study to validate the results of the mathematical model with experimental values, where a heat pump is utilized with a collector/evaporator of 1.65 m², ambient temperature between 27.1 and 31.6 °C, solar radiation between 0 and 811 W·m⁻², among other parameters, thanks to which the simulation generates a difference in the COP of 1.6 %, smaller than the experimental uncertainty of 5 %.

Likewise, the efficiency of the flat plate solar collectors may vary by the influence of other conditions such as the cross sections through which the working fluid circulates, as shown by Andrade *et al.* [9], who validate their research work by means of a CFD simulation; in addition, they show a final temperature of 330 K at the outlet of the pipe, and an efficiency of 68 %.

There are many research works about the use of solar collectors in heating systems, which are carried out in different countries, as shown in Table 1, where simulation proposals are validated experimentally for a more precise development.

Similarly, some works seek to numerically validate experimental proposals to find limitations in the design, which shows the importance of the complementarity between the simulation and experimental parts.

Table 1. Research works carried out in different systems with flat plate solar collectors

	Ji et al. [10]	Mohamed et al. [7]	Duarte et al. [8]	Fathabadi [11]	Rabelo et al. [12]	Kong et al. [13]
1. Type of solar collector						
Flat plate with cover	x	x	x	x		
Flat plate without cover					x	x
2. Application						
Hot sanitary water		x	x	x	x	x
Space heating	x					
3. Country	China	Sudán	Brasil	Grecia	Brasil	China
4. Area of the collector (m ²)	4	4.22	1.65	2.42	1.57	2.1
5. Length of the collector (m)	2	-	-	1.981	-	1.448
6. Validation	Experimental	Experimental and numerical	Experimental and numerical	Experimental	Experimental	Experimental

1.1. Description of the solar collector

The design of the equipment utilized for carrying out the present work consists of a tube, in which the energy exchange to the working fluid (water) takes place, covered with a metallic plate with two wings, as illustrated in Figure 1.



Figure 1. Schematic diagram of the solar collector

In pursuit of improving the heat transfer in the device, and thus considerably increasing its efficiency, the material considered in the model of the solar collector is copper for the metallic cover with the wings and the tube through which the working fluid circulates, with the dimensions specified in Table 2, taking into account the variables that directly impact on the temperature increase in the fluid, between the inlet and the outlet of the collector.

Table 2. Detailed specifications of the solar collector

Description	Specification
Length of the absorbing plate	0.960 m
Thickness of the absorbing plate	0.001 m
Thermal conductivity of the plate	387.6 W·m ⁻¹ ·K ⁻¹
Density of the plate material	8978 kg·m ⁻³
Thickness of the plate	0.001 m
Diameter of the conductive tube	0.0165 m
Thickness of the incremental and conductive tube	0.002 m
Total area	1.728 m ²

1.2. Operating principle of the system

The working fluid begins its circulation through the system entering at ambient temperature (T_{amb}) in the solar collector, where as a result of the heat transferred by the solar energy (Q_E) it reaches a temperature at

the outlet (T_1) larger than at the inlet, then enters a tank where it loses part of the heat gained (Q_{P1}) until entering the pump where it gains work (W) to move to a second tank where it loses the remaining heat gained in the solar collector (Q_{P2}) and then reenters the solar collector at ambient temperature, as detailed in Figure 2.

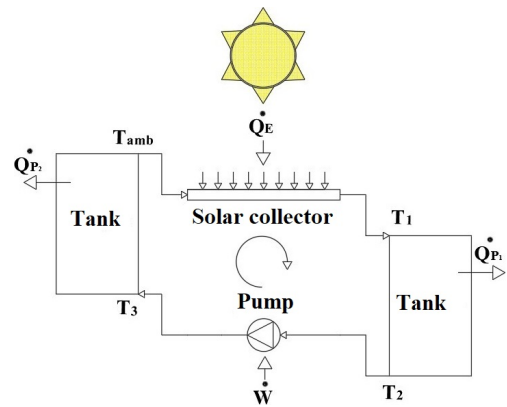


Figure 2. Cycle of the working fluid in the solar collector

2. Materials and methods

In a solar collector heat is transferred in three different ways: conduction, convection and radiation, which occur due to the solar radiation striking the device, and the temperature difference between the working fluid and the ambient air T_∞ , as seen in Figure 3.

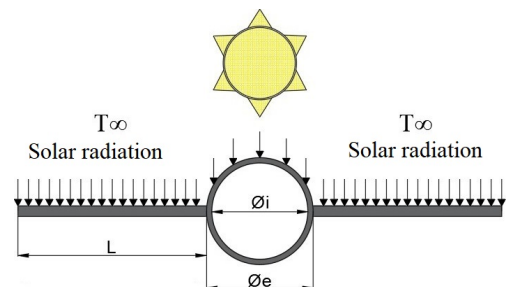


Figure 3. Heat transfer in a solar collector

Convection and radiation are due to the heat transfer through the ambient air up to the device surface, and to the solar energy received by the collector, respectively. On the other hand, conduction occurs due to the heat transfer between the solar collector surface, as shown in Figure 4.

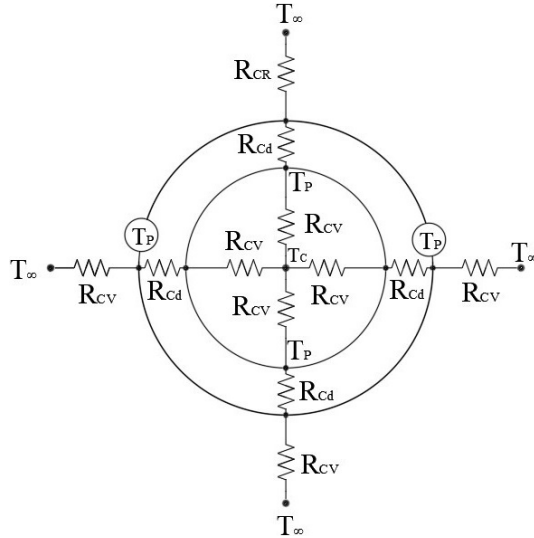


Figure 4. Network of thermal resistances in a solar collector

The heat transfer by conduction (q), explained by Fourier's law, is proportional to the temperature gradient (dT/dx) multiplied times the area (A) through which the energy is transferred; the relationship between the local temperature (T), the distance in the direction of heat flow (x) and the thermal conductivity (k) is shown in Equation (1) [14].

$$q = -k \cdot A \cdot \frac{dT}{dx} \quad (1)$$

The heat exchange by convection (Q_{cv}) for a model can be expressed as the process of heat convection between the internal and external surfaces of the envelope of a surface as expressed in Equation (2) [15].

$$\dot{Q}_{cv} = h \cdot A_S \cdot (T_S - T_\infty) \quad (2)$$

Where (h) represents the convection heat transfer coefficient, (A_S) the surface area, (T_S) the temperature of the surface and (T_∞) the temperature of the fluid at a certain distance of the surface. It should be considered that the temperature of the fluid is equal to the temperature on the surface of the solid in the contact area [16]. Regarding convection, it is important to classify it in two types: natural or free and forced.

The intensity of natural convection is measured by the Grashof (Gr) and Prandtl (Pr) number, which is shown in Equation (3), these dimensionless numbers are characteristic of free convection, since when they increase, the transition of the flow regime becomes insignificant as stated by Meyer and Everts [17].

$$Gr = \frac{g \cdot \vartheta \cdot \beta \cdot (T_2 - T_1) \cdot L^3}{\mu^2} \quad (3)$$

Where (g) represents the gravity, (ϑ) the density, (β) the volumetric expansion coefficient, (T_2 y T_1) are the temperatures at the boundary, (L) the wall length and (μ) the dynamic viscosity [18]. The free convection heat transfer can be quantified by means of the Nusselt number, which varies as a function of the conditions in which the heat exchange takes place, in this case of free convection, it is related to the dimensionless Rayleigh (Ra) number shown in Equation (4), which results from the product of the Grashof and Prandtl numbers [19].

$$Ra = \frac{g \cdot \beta \cdot (T_2 - T_1) \cdot R^3}{\nu \cdot \alpha} \quad (4)$$

For correct calculation of the Rayleigh number it is necessary to take into account the volumetric expansion coefficient, the temperature of the fluid (T_2), the temperature of the enclosure wall (T_1), the radius of the enclosure (R), the cinematic viscosity (ν) and the thermal diffusivity (α) [20]. The thermal radiation is the energy emitted by any type of matter which is at a temperature greater than zero and whose energy diffusion is shown in Equation (5), where it is presented [21].

$$q = k_a \cdot 4\sigma \cdot T^4 \quad (5)$$

Equation (5) presents the heat transfer of the radioactive source (q), the thermal conductivity (k_a), the Stefan-Boltzmann constant ($\sigma = 5.67 \times 10^{-8} W \cdot m^{-2} \cdot K^{-4}$) in units of the International System (SI) and the temperature distribution due to the limit of the physical media (T) [22].

2.1. Parameters of the fluid at the inlet of a flat solar collector

Some important conditions of the working fluid at the inlet of a flat solar collector were: velocity, mass flow, gauge pressure, ambient temperature, among others, as seen in Table 3, which have been collected from different research works that show the conditions at the inlet of a solar collector.

Table 3. Conditions of the fluid at the inlet of the solar collector

Properties	Cetina-Quiñones <i>et al.</i> [23]	Pang <i>et al.</i> [24]	Visa <i>et al.</i> [25]
Temperature	45 °C	27 °C	20 °C
Volumetric flow	0.0167 L · s ⁻¹	0.05 L · s ⁻¹	—
Pressure	—	—	300 kPa
Mass flow	—	0.1 kg · s ⁻¹	0.02 kg · s ⁻¹
Internal diameter	0.0254 mm	—	0.008 m
Working fluid	Water	Water	Water
Material of the pipe	—	Copper	Aluminum

2.2. Meshed and modeling

To correctly analyze the different properties of the solids, liquids and gases with the simulation software, it is necessary to construct an efficient computational mesh, which may be constituted by pyramidal, tetrahedral or hexahedral cells that divide the body in various smaller subsets [26]. To generate a correct mesh of the fluid section it is recommended to use tetrahedral cells due to their adaptability with the curved regions crossed by the fluid.

The independence of the meshed is important to determine the optimal mesh number, which means that the solution is independent of the mesh resolution. In the 3D CFD analysis it is common to carry out simulations using different mesh sizes to compare the results, despite this it is possible to find variations smaller than 0.5 % in the temperatures, which indicates that this does not have a significant impact on the results [27].

In the current case study it was required a differentiated meshed as illustrated in Figure 5. To obtain the mesh, a patch conforming tetrahedral method was utilized in the curved figures of the working fluid and of the tube that contains it, edge sizing along the joints between the wings and the arc in the collector wall with an angle of curvature of 5°, which is shown in Table 4 as mesh 1; in this way, typical hexahedrons and tetrahedrons are utilized in the CFD analysis of the solar collectors, heterogeneous distribution of its elements and different number of neighboring elements, which represent an unstructured meshed to improve the convergence of the result [28].

Due to the search for high reliability results it was necessary to establish an efficient meshed and, consequently, with a proper number of nodes and elements. However, a comparative analysis was carried out between a variety of meshes with different qualities and number of elements, as shown in Table 4, to verify the efficiency of the meshed in this work; as a result, the mesh 1 model was taken with the excellent ratings of quality previously pointed out.

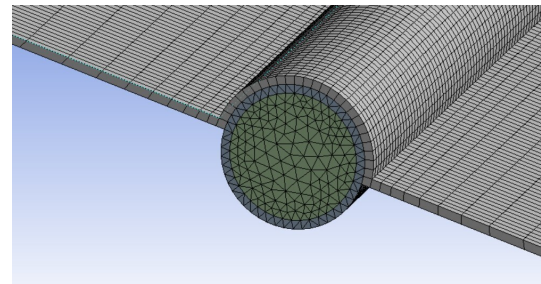


Figure 5. Mesh of the solar collector

Table 4. Types of meshes

Mesh	Number of elements	Skewness average
1	2272823	0.23763
2	149286	0.32162
3	92901	0.42708
4	192792	0.30576
5	247324	0.27664

With the help of the mesh quality, it can be seen in Figure 6 the different types of trends generated by the variability of results of the CFD simulation, which leads to the final selection of a particular meshed.

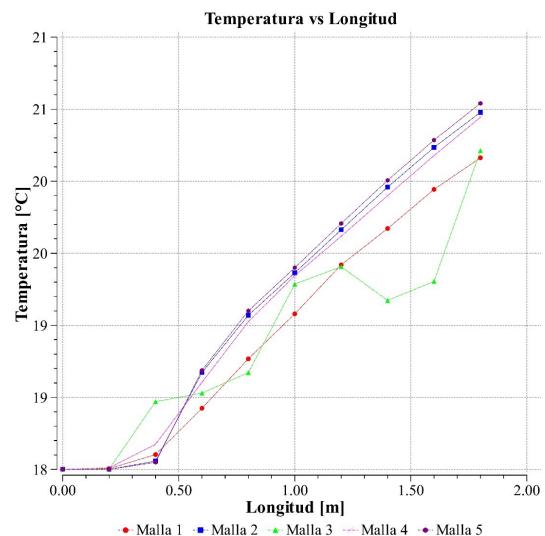


Figure 6. Variation of results with different meshed

To model the dynamic fluids, the CFD simulation software employs the Navier-Stokes equations, which

take into account the continuity, momentum and energy conservation, as shown in Equations (6), (7) and (8), respectively [29].

$$\frac{\partial \rho}{\partial t} + \nabla \cdot (\rho \vec{v}) = S_m \quad (6)$$

$$\begin{aligned} \frac{\partial \rho}{\partial t} (\rho \vec{v}) + \nabla \cdot (\rho \vec{v} \vec{v}) = \nabla p + \nabla \cdot [\mu \times (\nabla \vec{v} + \nabla \vec{v}^T)] + \\ + \rho \vec{g} + \vec{F} \end{aligned} \quad (7)$$

$$\frac{\partial \rho}{\partial t} (\rho E) + \nabla \cdot [\vec{v} \cdot (\rho E + p)] = \nabla \cdot (k_{eff} \cdot \nabla T) + S_h \quad (8)$$

When carrying out the validation of the CFD simulation results, it is important to know the permissible range of the variation that such results may exhibit with respect to the experimental values of the same study; this range can be measured with the percentage error presented in Equation 9, and according to different authors the maximum permissible value is 5.2 % [30].

$$Error \% = \frac{|X_{sim} - X_{exp}|}{X_{sim}} \quad (9)$$

3. Results and discussion

The radiation module of the CFD simulation software, solar calculator, enabled the analysis of the flat plate solar collector with parameters of latitude (-0.225219), longitude (-78.5248) and different hours to determine parameters such as surface temperature of the heat transfer device, as shown in Figure 7 (a and b) with hours from 11:00 to 12:00, respectively, where it is possible to observe a greater temperature distribution due to the radiation peak existing at 12:00 with a maximum value of $27.12 \text{ }^\circ\text{C}$; this temperature attenuates as time goes on as it is indicated by a smaller value of $24.63 \text{ }^\circ\text{C}$ on the wing surface at 13:00.

The radiation striking on the collector is directly related with the hours at which the test is conducted, as can be observed in Figure 8 (a and b), generating peak values between 12:00 and 13:15 with available radiation values between 650 and $800 \text{ W}\cdot\text{m}^{-2}$, respectively, influencing in a similar manner on the ambient temperature, a very important parameter in the heat transfer to the device and in its performance.

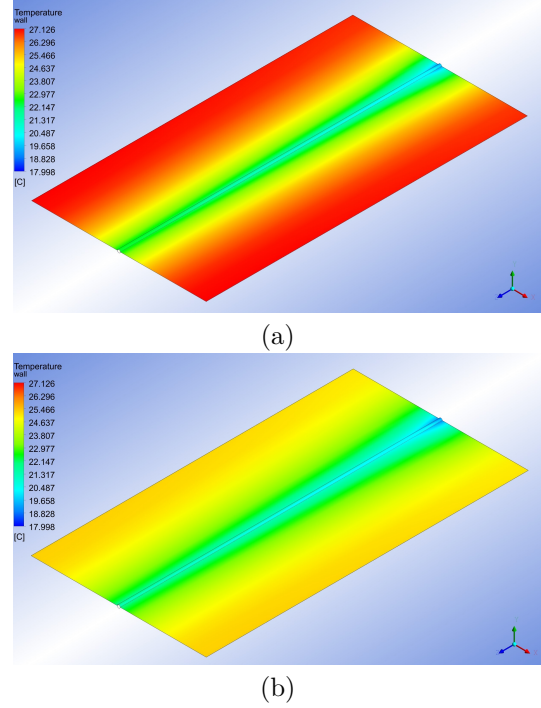


Figure 7. Temperature in the external wall of the solar collector

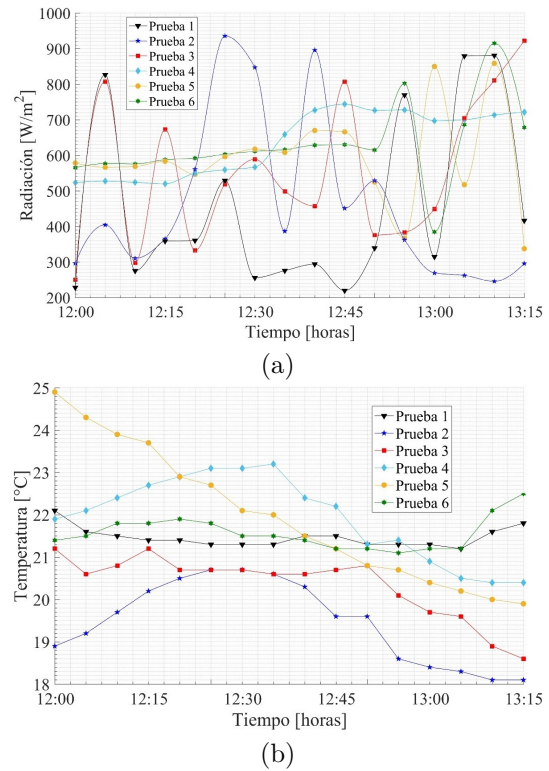


Figure 8. Variation of a) Radiation, b) Temperature

Due to the common variations of the radiation levels that fluctuate between 350 and $800 \text{ W}\cdot\text{m}^{-2}$ in the zone with the previously established latitude and longitude, along with the temperature and heat flow

change on the surface of the heat transfer device, it is possible to observe a greater temperature at the center of the working fluid along the center of the tube in the solar collector at specific times, as illustrated in Figure 9, and due to this it is determined that the largest temperature at the outlet of the collector will occur at 12:00 with a value of 20.2 °C and with the smallest value of 18.65 °C at 10:00 when going across the total length of the flat plate heat exchanger.

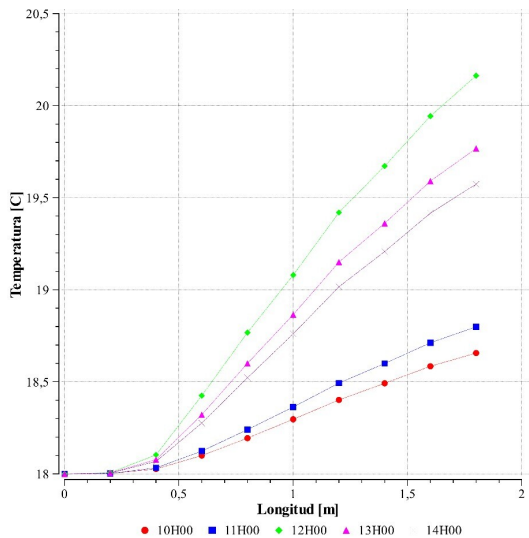
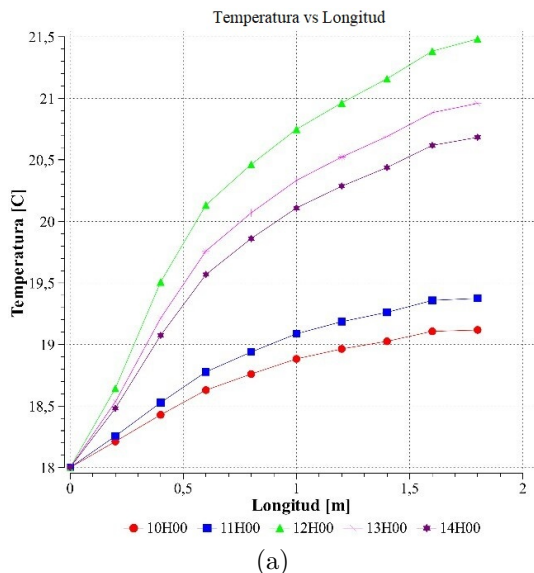
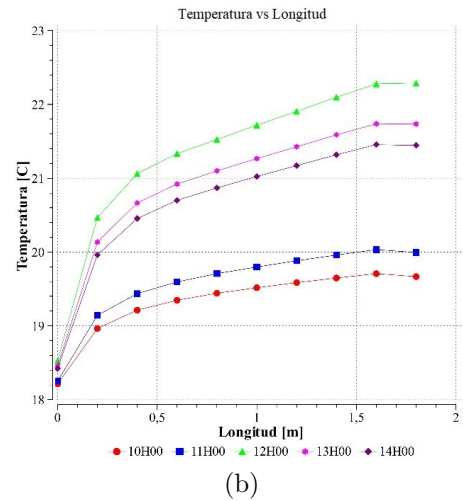


Figure 9. Comparative diagram of temperature vs. length at the center of the collector

It is possible to observe a greater temperature increase as the fluid approaches the tube wall in the heat exchanger, as it is appreciated in Figure 10(a), where the temperature is measured along the solar collector in an intermediate space between the wall and the center of the tube, and additionally Figure 10(b) illustrates the temperature variation in the collector wall.



(a)



(b)

Figure 10. Comparative diagrams of temperature vs. length at a) ¼ of the surface, b) surface

The results of the CFD simulation presented in Figure 9 show the same trend that the experimental results, as can be observed in Figure 11, validating the results within an error margin of 4.01 % in the analysis at the center of the solar collector at the different hours.

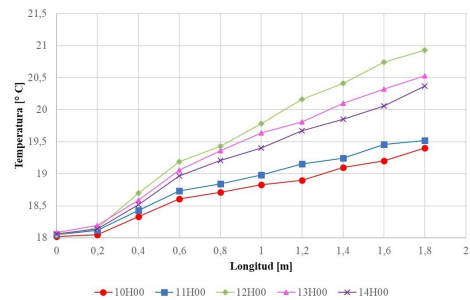


Figure 11. Comparative diagrams of temperature vs. length with experimental results

When carrying out the comparative analysis between the experimental results and the results of the numerical simulation, it is possible to find a similar trend in both cases as shown in Figure 12. Similarly, it is possible to appreciate a maximum percentage error of 4.01 %, thus validating the experimental and simulation data.

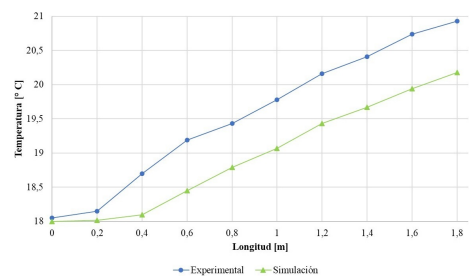


Figure 12. Comparative diagram in the experimental and numerical analysis at 12:00

4. Conclusions

In the present study an analysis of the performance of a flat plate solar collector was performed by means of a CFD simulation software, where the solar radiation at different hours has been utilized in several simulations carried out; such radiation directly influences the transfer of thermal energy to the working fluid, showing various results.

The maximum value of fluid temperature at the outlet of the solar collector is 20.16 °C at 12:00, while the smallest fluid temperature at the outlet was obtained at 10:00 with 18.65 °C, due to the low solar radiation at that time; these values represent a favorable trend for the utilization of the fluid in different processes, all this without ruling out the use of independent fluid heating processes to reach a specific temperature in the search for fulfilling a particular need.

The radiation peak occurring at 12:00 generates a maximum heat flow of 96.02 W·m⁻² to the working fluid, thus achieving the maximum amount of energy transfer in all the analysis range considered in the research. It is possible to appreciate a temperature variation on the external surface of the heat transfer device in accordance with the typical radiation levels at the different hours under study, obtaining a maximum value of 27.12 °C and a minimum value of 20.48 °C at 12:00 and 10:00, respectively. At last, it can be verified that the simulation and experimental data differ 4.01 % when compared to each other.

Acknowledgment

The authors thank the Universidad Politécnica Salesiana, Universidad Pontificia Bolivariana and the «Energética 2030» alliance (Research Program with code No. 58667), for the call «778-2017 Scientific Ecosystem» of COLCIENCIAS, financed by the World Bank. The research program is administered by the Ministerio de Ciencia, Tecnología e Innovación (Minciencias) through contract No. FP44842-210-2018.

References

[1] L. Evangelisti, R. D. L. Vollaro, and F. Asdrubali, “Latest advances on solar thermal collectors: A comprehensive review,” *Renewable and Sustainable Energy Reviews*, vol. 114, p. 109318, 2019. [Online]. Available: <https://doi.org/10.1016/j.rser.2019.109318>

[2] J. Calle-Sigüencia and O. Tinoco-Gómez, “Obtención de ACS con energía solar en el cantón Cuenca y análisis de la contaminación ambiental,” *Ingenius*, no. 19, pp. 89–101, 2018. [Online]. Available: <https://doi.org/10.17163/ings.n19.2018.09>

[3] L. M. Ayompe and A. Duffy, “Analysis of the thermal performance of a solar water heating system with flat plate collectors in a temperate climate,” *Applied Thermal Engineering*, vol. 58, no. 1, pp. 447–454, 2013. [Online]. Available: <https://doi.org/10.1016/j.applthermaleng.2013.04.06>

[4] W. M. Hashim, A. T. Shomran, H. A. Jurmut, T. S. Gaaz, A. A. H. Kadhum, and A. A. Al-Amiery, “Case study on solar water heating for flat plate collector,” *Case Studies in Thermal Engineering*, vol. 12, pp. 666–671, 2018. [Online]. Available: <https://doi.org/10.1016/j.csite.2018.09.002>

[5] E. Arteaga-López, C. Ángeles-Camacho, and F. Bañuelos-Ruedas, “Advanced methodology for feasibility studies on building-mounted wind turbines installation in urban environment: Applying CFD analysis,” *Energy*, vol. 167, pp. 181–188, 2019. [Online]. Available: <https://doi.org/10.1016/j.energy.2018.10.191>

[6] A. Marroquín-De Jesús, J. M. Olivares-Ramírez, O. Jiménez-Sandoval, M. A. Zamora-Antuñano, and A. Encinas-Oropesa, “Analysis of flow and heat transfer in a flat solar collector with rectangular and cylindrical geometry using CFD,” *Ingeniería, Investigación y Tecnología*, vol. 14, no. 4, pp. 553–561, 2013. [Online]. Available: [https://doi.org/10.1016/S1405-7743\(13\)72265-0](https://doi.org/10.1016/S1405-7743(13)72265-0)

[7] E. Mohamed, S. Riffat, S. Omer, and R. Zeinelabdein, “A comprehensive investigation of using mutual air and water heating in multi-functional dx-sahp for moderate cold climate,” *Renewable Energy*, vol. 130, pp. 582–600, 2019. [Online]. Available: <https://doi.org/10.1016/j.renene.2018.06.075>

[8] W. M. Duarte, T. F. Paulino, J. J. G. Pabón, S. Sawalha, and L. Machado, “Refrigerants selection for a direct expansion solar assisted heat pump for domestic hot water,” *Solar Energy*, vol. 184, pp. 527–538, 2019. [Online]. Available: <https://doi.org/10.1016/j.solener.2019.04.027>

[9] A. X. Andrade Cando, W. Quitiaquez Sarzosa, and L. F. Toapanta, “CFD analysis of a solar flat plate collector with different cross sections,” *Enfoque UTE*, vol. 11, no. 2, pp. 95–108, 2020. [Online]. Available: <https://doi.org/10.29019/enfoque.v11n2.601>

[10] W. Ji, J. Cai, J. Ji, and W. Huang, “Experimental study of a direct expansion solar-assisted heat pump (dx-sahp) with finned-tube evaporator and comparison with conventional dx-sahp,” *Energy and Buildings*, vol. 207, p. 109632, 2020. [Online]. Available: <https://doi.org/10.1016/j.enbuild.2019.109632>

- [11] H. Fathabadi, “Novel low-cost parabolic trough solar collector with tpct heat pipe and solar tracker: Performance and comparing with commercial flat-plate and evacuated tube solar collectors,” *Solar Energy*, vol. 195, pp. 210–222, 2020. [Online]. Available: <https://doi.org/10.1016/j.solener.2019.11.057>
- [12] S. N. Rabelo, T. de F. Paulino, W. M. Duarte, S. Sawalha, and L. Machado, “Experimental analysis of the influence of water mass flow rate on the performance of a co2 direct-expansion solar assisted heat pump,” *International Journal of Chemical and Molecular Engineering*, vol. 12, no. 7, pp. 327–331, 2018. [Online]. Available: <https://doi.org/10.5281/zenodo.1317384>
- [13] X. Kong, P. Sun, S. Dong, K. Jiang, and Y. Li, “Experimental performance analysis of a direct-expansion solar-assisted heat pump water heater with r134a in summer,” *International Journal of Refrigeration*, vol. 91, pp. 12–19, 2018. [Online]. Available: <https://doi.org/10.1016/j.ijrefrig.2018.04.021>
- [14] J. Lee and T.-H. Song, “Conduction/radiation combined heat transfer with contact resistance for application to vacuum insulation,” *International Journal of Heat and Mass Transfer*, vol. 129, pp. 380–388, 2019. [Online]. Available: <https://doi.org/10.1016/j.ijheatmasstransfer.2018.09.085>
- [15] F. Jiang, Z. Li, Q. Zhao, Q. Tao, S. Lu, and K. Zhao, “The influence of exterior louver blinds’ geometric and thermal attributes on the convective heat transfer at building facades,” *Solar Energy*, vol. 193, pp. 654–665, 2019. [Online]. Available: <https://doi.org/10.1016/j.solener.2019.09.074>
- [16] Y. Zhang, J. Wang, W. Liu, and Z. Liu, “Heat transfer and pressure drop characteristics of r134a flow boiling in the parallel/tandem microchannel heat sinks,” *Energy Conversion and Management*, vol. 148, pp. 1082–1095, 2017. [Online]. Available: <https://doi.org/10.1016/j.enconman.2017.06.067>
- [17] J. P. Meyer and M. Everts, “Chapter three - a review of the recent developments in laminar, transitional, quasi-turbulent and turbulent forced and mixed convective flow through horizontal tubes,” in *Advances in Heat Transfer*, ser. Advances in Heat Transfer, E. M. Sparrow, J. P. Abraham, J. M. Gorman, and W. Minkowycz, Eds. Elsevier, 2019, vol. 51, pp. 131–205. [Online]. Available: <https://doi.org/10.1016/bs.aiht.2019.07.001>
- [18] S. MOJUMDER, S. A. H. A. Sourav, S. A. H. A. Sumon, and M. A. H. MAMUN, “Combined effect of reynolds and grashof numbers on mixed convection in a lid-driven t-shaped cavity filled with water-al2o3 nanofluid,” *Journal of Hydrodynamics, Ser. B*, vol. 27, no. 5, pp. 782–794, 2015. [Online]. Available: [https://doi.org/10.1016/S1001-6058\(15\)60540-6](https://doi.org/10.1016/S1001-6058(15)60540-6)
- [19] P. Sánchez-Palencia, N. Martín-Chivelet, and F. Chenlo, “Modelización del coeficiente de transmitancia térmica de módulos fotovoltaicos para integración en edificios,” in *XVI Congreso Ibérico y XII Congreso Iberoamericano de Energía Solar*, 2018. [Online]. Available: <https://bit.ly/2C4petH>
- [20] N. Rahbar, J. A. Esfahani, and E. Fotouhi-Bafghi, “Estimation of convective heat transfer coefficient and water-productivity in a tubular solar still - CFD simulation and theoretical analysis,” *Solar Energy*, vol. 113, pp. 313–323, 2015. [Online]. Available: <https://doi.org/10.1016/j.solener.2014.12.032>
- [21] C.-H. Wang, Y.-Y. Feng, K. Yue, and X.-X. Zhang, “Discontinuous finite element method for combined radiation-conduction heat transfer in participating media,” *International Communications in Heat and Mass Transfer*, vol. 108, p. 104287, 2019. [Online]. Available: <https://doi.org/10.1016/j.icheatmasstransfer.2019.104287>
- [22] B. P. Jelle, S. E. Kalnes, and T. Gao, “Low-emissivity materials for building applications: A state-of-the-art review and future research perspectives,” *Energy and Buildings*, vol. 96, pp. 329–356, 2015. [Online]. Available: <https://doi.org/10.1016/j.enbuild.2015.03.024>
- [23] A. J. Cetina-Quiñones, A. Bassam, G. Hernández-Chan, I. Hernández Benítez, J. Hernández Reyes, and D. Lugo Chávez, “Modelación térmica de un colector solar de canal parabólico mediante el método de elementos finitos,” *Ingeniería*, vol. 21, no. 1, pp. 1–12, 2017. [Online]. Available: <https://bit.ly/2MYMg7D>
- [24] W. Pang, Y. Cui, Q. Zhang, G. J. Wilson, and H. Yan, “A comparative analysis on performances of flat plate photovoltaic/thermal collectors in view of operating media, structural designs, and climate conditions,” *Renewable and Sustainable Energy Reviews*, vol. 119, p. 109599, 2020. [Online]. Available: <https://doi.org/10.1016/j.rser.2019.109599>
- [25] I. Vișa, M. Moldovan, and A. Duță, “Novel triangle flat plate solar thermal collector for facades integration,” *Renewable Energy*, vol. 143, pp. 252–262, 2019. [Online]. Available: <https://bit.ly/30Jsxkr>

- [26] D. H. Lobón, E. Baglietto, L. Valenzuela, and E. Zarza, “Modeling direct steam generation in solar collectors with multiphase CFD,” *Applied Energy*, vol. 113, pp. 1338–1348, 2014. [Online]. Available: <https://doi.org/10.1016/j.apenergy.2013.08.046>
- [27] A. Aghagoli and M. Sorin, “Thermodynamic performance of a CO₂ vortex tube based on 3d CFD flow analysis,” *International Journal of Refrigeration*, vol. 108, pp. 124–137, 2019. [Online]. Available: <https://doi.org/10.1016/j.ijrefrig.2019.08.022>
- [28] Z. Badiei, M. Eslami, and K. Jafarpur, “Performance improvements in solar flat plate collectors by integrating with phase change materials and fins: A CFD modeling,” *Energy*, vol. 192, p. 116719, 2020. [Online]. Available: <https://doi.org/10.1016/j.energy.2019.116719>
- [29] L. Zhou, Y. Wang, and Q. Huang, “CFD investigation of a new flat plate collector with additional front side transparent insulation for use in cold regions,” *Renewable Energy*, vol. 138, pp. 754–763, 2019. [Online]. Available: <https://doi.org/10.1016/j.renene.2019.02.014>
- [30] D. G. Gunjo, P. Mahanta, and P. S. Robi, “CFD and experimental investigation of flat plate solar water heating system under steady state condition,” *Renewable Energy*, vol. 106, pp. 24–36, 2017. [Online]. Available: <https://doi.org/10.1016/j.renene.2016.12.041>